

Streaming from the Air: Enabling High Data-rate 5G Cellular Links for Drone Streaming Applications

Lorenzo Bertizzolo^{†‡}, Tuyen X. Tran[‡], John Buczek[†],
 Bharath Balasubramanian[‡], Rittwik Jana[‡], Yu Zhou[‡], and Tommaso Melodia[†]
[†] Institute for The Wireless IoT, Northeastern University, Boston, MA, USA; [‡] AT&T Labs Research, Bedminster, NJ, USA
 {bertizzolo.l,buczek.j,melodia}@northeastern.edu,{tuyen,bharathb,rjana,yuzhou}@research.att.com

ABSTRACT

Enabling high data-rate uplink cellular connectivity for drones is a challenging problem, since a flying drone has a higher likelihood of having line-of-sight propagation to base stations that terrestrial UEs normally do not have line-of-sight to. This may result in uplink inter-cell interference and uplink performance degradation for the neighboring ground UEs when drones transmit at high data-rates (e.g., video streaming). We address this problem from a cellular operator's standpoint to support drone-sourced video streaming of a point of interest. We propose a low-complexity, closed-loop control system for Open-RAN architectures that jointly optimizes the drone's location in space and its transmission directionality to support video streaming and minimize its uplink interference impact on the network. We prototype and experimentally evaluate the proposed control system on an outdoor multi-cell RAN testbed. Furthermore, we perform a large-scale simulation assessment of the proposed system on the actual cell deployment topologies and cell load profiles of a major US cellular carrier. The proposed Open-RAN-based control achieves an average 19% network capacity gain over traditional BS-constrained control solutions and satisfies the application data-rate requirements of the drone (e.g., to stream an HD video).

KEYWORDS

UAV Communications; Aerial UE; Cellular Networks; 5G.

ACM Reference Format:

Lorenzo Bertizzolo^{†‡}, Tuyen X. Tran[‡], John Buczek[†], Bharath Balasubramanian[‡], Rittwik Jana[‡], Yu Zhou[‡], and Tommaso Melodia[†]. 2018. Streaming from the Air: Enabling High Data-rate 5G Cellular Links for Drone Streaming Applications. In *Proceedings of ACM Conference (Conference'17)*. ACM, New York, NY, USA, 10 pages. <https://doi.org/10.1145/1122445.1122456>

1 INTRODUCTION

Drones (or "UAVs") enable a wide range of new services and applications such as aerial surveillance, infrastructure monitoring, environmental sensing, transportation and delivery of goods, and live broadcast coverage [1, 3, 13, 15, 29]. Employing drones for

these applications can significantly lower the chance for human operators' injuries and reduce the overall operational cost when compared to larger form-factor solutions such as helicopters. To support beyond visual-line-of-sight control, drones are often equipped with on-board cellular user-equipment (UEs). Thanks to the cellular network coverage and support for broadband data-rates, drones can now be remotely operated over the Internet at unprecedented distances. At the same time, they can connect to remote broadcast servers and upload live video streams, such as live footage captured via on-board cameras, over the air-to-ground (A2G) cellular links. Unlike traditional terrestrial UEs that are typically situated at pedestrian heights, the UAV-based UEs operate at high altitudes and therefore in LoS condition with multiple (serving and neighboring) cellular base stations (BSs). While this condition is favorable for the drone [10], its transmitted signal will also propagate to multiple neighboring BSs, resulting in severe uplink inter-cell interference and uplink performance degradation for the ground UEs served by these BSs [7]. This problem is exacerbated when the drones transmit at high data-rates, for example, when streaming HD videos. As drone-sourced video streaming is a major application of interest, industries are posing significant pressure on network operators to support high bandwidth drone uplink communications in future 5G networks [2, 5]. To address this problem, the use of directional transmitters on UAVs, as opposed to omni-directional transmitters equipped on most UEs today, has been suggested as a practical method to constrain the transmitted signal power to one direction and limit the energy dispersion toward other neighboring BSs [7, 10, 25].

The need for drone cellular support was first introduced by the 3GPP in release 15 and carried on successive releases for operations in the 5G NR low- and mid-band (i.e., sub-6 GHz) [2]. At the same time, the O-RAN Alliance, a consortium of industry and academic partners, introduced important innovations for 5G Open-RAN architectures. Among these, the Open-RAN Intelligent Controller (RIC). This new architectural component provides a centralized abstraction of the RAN and facilitates custom control plane functions e.g., enabling closed-control via action and feedback loops between RAN components and their controllers[4]. *In this work, we exploit the architectural advantage of Open-RAN architectures and the practicality of using directional transmitters on a UAV to design a closed-loop control system that jointly optimizes the locations and transmission directionality of the UAV to satisfy its application requirements without penalizing the neighboring ground users.* We envision an application scenario where the UAV is interested in capturing and streaming the live footage of a particular event or

Permission to make digital or hard copies of all or part of this work for personal or classroom use is granted without fee provided that copies are not made or distributed for profit or commercial advantage and that copies bear this notice and the full citation on the first page. Copyrights for components of this work owned by others than ACM must be honored. Abstracting with credit is permitted. To copy otherwise, or republish, to post on servers or to redistribute to lists, requires prior specific permission and/or a fee. Request permissions from permissions@acm.org.
Conference'17, July 2017, Washington, DC, USA

© 2018 Association for Computing Machinery.
 ACM ISBN 978-x-xxxx-xxxx-x/YY/MM...\$15.00
<https://doi.org/10.1145/1122445.1122456>

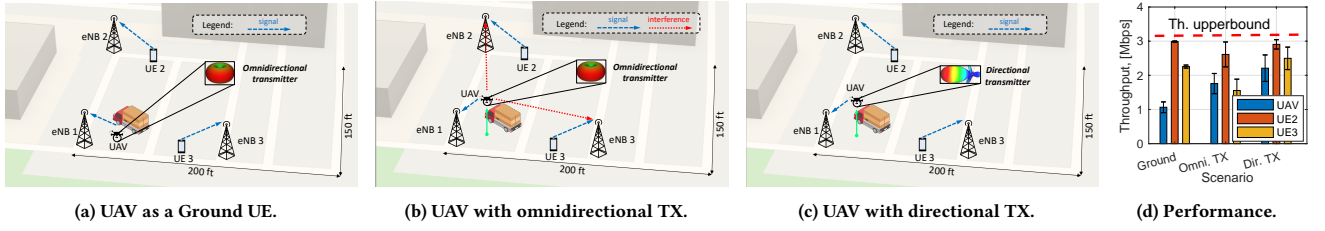


Figure 1: Motivation cellular network deployment: 3-eNBs serving 2 UEs and one UAV-based UE employing different antenna patterns.

object located at a Point of Interest (POI). The drone would contact the control service running at the cellular infrastructure for instructions regarding the optimal aerial location and transmission directionality that satisfy the application's requirements.

Specifically, we make the following contributions:

- To motivate this work, we quantify the ground UEs' uplink throughput degradation (as much as 20%), in the presence of a drone on a dedicated full-stack cellular testbed. Moreover, we verify how controlling the drones' location and transmission directionality can improve the overall network performance (up to 28%).
- We mathematically formulate the network control problem of a drone streaming video from a POI. Due to difficulty for the drone to physically relocate and adapt to the fast-changing dynamics of the involved network variables (e.g., radio resource scheduling and modulation schemes, which vary at the timescale of milliseconds), we reformulate the original problem using long-term average network information such as cell load and average UEs' uplink signal power. We propose a closed-loop control solution for Open-RAN architectures specifically for the coexistence of one aerial and terrestrial UEs. Our system features *low overhead*, in-band communication (which makes it *backwards compatible*) and operates on a drone-initiated request-based approach that guarantees *users' privacy*.
- We prototype the proposed control solution in a real outdoor, multi-BS RAN cellular testbed. Through extensive experiments, we demonstrate that our Open-RAN-based control achieves 26% network capacity gain compared to traditional intra-cell optimization. To the best of our knowledge, this is the first full-stack experimental assessment of intelligent control for cellular-enabled UAVs.
- Further, we assess the performance of our solution at scale through extensive simulations using commercial cell topology and cell load profiles from a major US cellular operator for various scenarios. We show the *effectiveness* (an average 20% network capacity gain), *adaptability*, and *scalability* of our control approach.

The remainder of the paper is organized as follows. Section 2 motivates the need for a drone-specific control system through real-world measurements. Section 3 formulates the drone-specific network control problem we aim to solve. Section 4 proposes the design of a closed-loop control system for Open-RAN architectures. The proposed approach is assessed through real-world experiments and extensive simulations in Section 5. We summarize the related work in Section 6 and draw the main conclusions in Section 7.

2 MOTIVATIONAL EXPERIMENTS

To motivate the need for a UAV-specific control solution we perform a first-of-its-kind measurement campaign on a dedicated outdoor full-stack LTE testbed with a mixed set of aerial and ground UEs. Specifically, we aim to assess the ground UEs' *uplink* performance

degradation caused by one UAV connected to a different cell, as we vary the UAV's location, antenna pattern, and transmission directionality. Our LTE-based analysis adopts the same 5G low- and mid-band frequencies designated for drone cellular links (FR1).

2.1 UAV- and Terrestrial-UEs Coexistence

Our testbed consists of three cells (eNBs), each serving one cellular user (UE) as illustrated in Fig. 1. We refer the reader to Section 5.1 for a detailed description of the experimental setup, including the software, hardware, and testing methodology. Here, we analyze three scenarios: Ground UAV: the UAV acts as a traditional ground UE with an obstacle (a big van) positioned to mimic the typical blockage experienced by pedestrians (Fig. 1a). The drone should be considered as a traditional ground user for this case. Omnidirectional TX: The UAV-based UE is an aerial user flying higher than the obstacle height, employing a traditional omnidirectional antenna (Fig. 1b). Directional TX: The UAV-based UE is an aerial user flying higher than the obstacle height, employing a directional antenna pointing at its serving BS (Fig. 1c).

First, we assess the performance of the overall network in the absence of aerial links, that is when all the UEs are on the ground. In this case, we do not fly the drone and keep it behind the positioned obstacle (see Fig. 1a). For each experiment in this section, we repeat a 10 second(s)-long measurement for 20 times and record the per-user uplink throughput and its standard deviation in Megabits per second (Mbps). The network performance for the first experiment is reported in Fig. 1d ('Ground'). To better quantify the interference dynamics, we also measure the single-user upper-bound performance measured in isolation, that is, when no other users are present in the network. We report this as the red dashed line in Fig. 1d. In absence of a flying UE, the average per-user uplink throughput is 2.1 Mbps, while the aggregate network throughput is 6.3 Mbps. Next, we assess the performance of our network when flying the UAV-based user. In this scenario, the UAV-based user hovers above the obstacle height, and thus benefits from the LoS condition with multiple eNBs as shown in Fig. 1b. We measure the network performance and report them in Fig. 1d ('Omni. TX'). The aerial LoS favors the UAV which records 1.76 Mbps (+65% over the 'Ground' scenario), however, the performance of UE 1 and UE 2 drop to 2.61 Mbps (−12%) and 1.55 Mbps (−31%), respectively. Despite slightly favoring the UAV, this scenario degrades the performance of neighboring cells by 20% compared to the 'Ground' scenario.

In our third deployment, the UAV is flying above the obstacle height (as in Fig. 1c) is equipped with a steerable directional transmitter (directional antenna) pointed toward the dominant LOS path with the serving eNB. We record the average per-user uplink throughput of 2.2 Mbps and the aggregate network performance

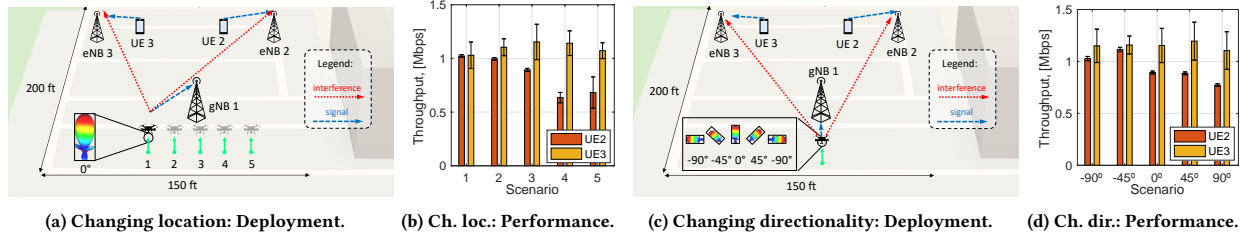


Figure 2: Measurements for different UAV locations (and same TX directionality) and different TX directionality (and same location).

of 7.6 Mbps as reported in Fig. 1d to the right ('Dir. TX'). Equipping the UAV with a directional transmitter benefits the UAV itself (+25% throughput as compared to the 'Omnidirectional TX' scenario) and the other UEs as well (+11% and +60%, respectively). Overall, employing a directional transmitter at the UAV increases the UAV data-rate by 28% and reduces the inter-cell interference by 30% with respect to the 'Omnidirectional TX' scenario.

2.2 Effect of UAV Parameters

Here, we measure and observe how the performance of the prototyped cellular network varies with the UAV's location and its transmission directionality. We treat the two cases in isolation.

Changing the UAV's Location. Figs. 2b and 2b report the deployment and performance of the 3-eNB RAN network for the UAV at 5 different locations, connected to eNB 1. As the UAV moves to 5 different locations, UE 2 and UE 3 experienced uplink rate variation of up to 30%. This experiment suggests that the UAV location can be controlled to tune the UAV impact on the rates of the neighboring ground users.

Changing the UAV's TX Directionality. Figs. 2d and 2d show the deployment and performance as we fix the UAV's location and vary its transmission directions, namely -90° , -45° , 0° , 45° , and 90° with respect to its LOS direction with its serving eNB. The 5 UAV transmission directions correspond to different UE 2 and UE 3 rates with variations up to 38%. This experiment suggests that the UAV transmission directionality can be controlled to tune the UAV impact on the neighboring ground users' rate.

In conclusion, through real-world experiments, we have verified the considerable implications of extending cellular support to aerial users, specifically in terms of the throughput degradation faced by the ground users. In this article, we experimentally verify for the first time that employing directional transmitters at a UAV can bring significant performance improvements to the overall network, both in terms of overall network performance (+28%) and throughput degradation to the rest of the network (-30%). These statistics, applied to a commercial 5G cellular network with full operational bandwidth and dense deployment translate into a per-user throughput degradation up to 20 Mbps for a single connected UAV in the surrounding. Finally, we demonstrate that UAV location and directionality can be controlled to adjust the experienced rates of neighboring ground users. With this premise, we study new solutions to enable optimized aerial cellular communications.

3 CONNECTED-DRONE CONTROL PROBLEM

In this section, we formally define and mathematically formulate the specific Connected-Drone Control Problem (CDCP) of a drone intending to stream video content from nearby a Point of Interest

(POI). Then, we iterate over the formulation and simplify its parameters to be observable and easily retrievable. Finally, we explain how to solve the newly formulated problem via global optimization.

3.1 CDCP Formulation

Alongside the 3GPP's directives, suggesting drones operations in the 5G NR low- and mid-band (i.e., sub-6 GHz), we herein consider the signal propagation characteristics of sub-6 GHz spectrum [2]. Accordingly, we consider a small region in a traditional cellular network deployment where a set of Base Stations (BSs) \mathcal{J} , serve multiple ground cellular users denoted by the set \mathcal{I} . Specifically, each BS $j \in \mathcal{J}$ serves a finite number of users denoted by the set \mathcal{I}_j , where the different sets \mathcal{I}_j are disjoint, i.e., $\mathcal{I}_j \cap \mathcal{I}_i = \emptyset \forall i \neq j$. Let us denote the number of UEs served by BS j as $w_j = |\mathcal{I}_j|$. Additionally, there is a UAV-based user, denoted by u that is served by BS $j_u \in \mathcal{J}$ as illustrated in Fig. 3a. Accordingly, $w_u = |\mathcal{I}_u| + 1$ when the UAV is present. At any given time, a cellular UE is allocated a finite number of uplink and downlink Physical Resource Blocks (PRBs) by the 5G BS scheduler. A PRB is the minimum bandwidth resource unit, corresponding to 12 subcarriers, that can be allocated to a user. At a given time instant, let us indicate with x_i the number of *uplink* PRBs allocated to user i . For the sake of formulation, we assume that all the cells operate on the same carrier frequency band with bandwidth B , and each user i is allocated a bandwidth B_i that equals x_i times the bandwidth of a PRB B_{PRB} . Hereafter, all traffic analysis implicitly refers to uplink traffic only.

As per the 5G New Radio (NR) physical layer specification, cellular users' uplink channel access happens in Cyclic Prefix Orthogonal Frequency-division Multiplexing (CP-OFDM) or Discrete Fourier Transform Spread Orthogonal Frequency Division Multiplexing (DFT-s-OFDM). In this specification, when the cellular users access channels with overlapping frequencies, they interfere with each other as reported in Fig. 3b. As we discussed and experimentally demonstrated in the 'Ground' scenario in the previous section (§2), the impact of ground UEs-generated interference on other ground users is marginal as their uplink power to neighboring cells is attenuated by surrounding obstacles such as buildings, vehicles, or trees. It is instead a more serious issue when the interference comes from drones up in the sky.

Let us define x_{iu} as the number of uplink PRBs that user i served by BS j_i is co-scheduled with those of the UAV served by BS j_u . The x_{iu} parameters are integer numbers that equal zero when the ground user i has no shared resource allocation with the UAV u , e.g., $x_{iu} = 0$ for $i = 1, 6$, and are non-zero positive integers otherwise, e.g., $x_{iu} > 0$ for $i = 2, 3, 4, 5$ (see Fig. 3b). Due to the orthogonality of intra-cell scheduling decisions, it is guaranteed that $x_{iu} = 0$ for all the users that are in the same cell j_u serving the UAV, e.g.,

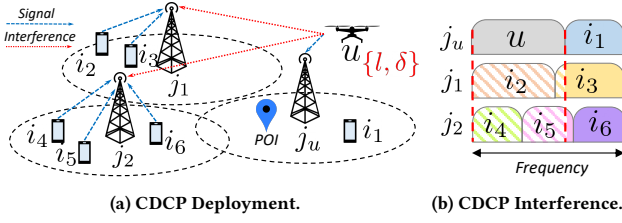


Figure 3: Connected-Drone Control Problem (CDCP) scenario.

for $i = 1$, while $x_{iu} > 0$ for at least one user i served by the cell $j_i \neq j_u$, that is, $\sum_{i \in \mathcal{I}_j} x_{iu} > 0 \forall j \neq j_u \in \mathcal{J}$. Last, we normalize the coefficients x_{iu} as $\hat{x}_{iu} = x_{iu}/x_i$. The coefficients $\hat{x}_{iu} \in [0, 1]$ represent the band share that user i has with the UAV u . Similarly, $\hat{x}_{ui} = x_{ui}/x_u$ represent the UAV band share with the ground user i . Let us define the uplink signal power of user i received at the serving BS j_i as P^i and the received signal power of the UAV at its serving BS j_u as $P^u(l, \delta)$, function of the UAV's location $l \in \mathcal{L}$, where \mathcal{L} is the set of possible 3D locations in space, and the 3D transmission direction $\delta = (\delta_a, \delta_e) \in \{[0, 2\pi], [0, \pi]\}$, where δ_a and δ_e are the azimuth and elevation directions. Similarly, $P_j^u(l, \delta)$ denotes the UAV's uplink interference power at cell $j \neq j_u$. The received UAV's power at a BS j is calculated through

$$P_j^u(l, \delta) = P_{TX}^u - L_{PL}(l, l_j) + G_{Dir}(\delta, l_j) \quad (1)$$

where P_{TX}^u is the UAV transmitted power (maximum 23 dBm for 5G UEs), $G_{Dir}(\delta, l_j)$ is the angular gain of the employed directional transmitter with respect to the BS's j location l_j , and $L_{PL}(l, l_j)$ is the uplink Air-to-Ground (A2G) path-loss attenuation among the two locations l and l_j . The latter is inclusive of effects such as BS antenna's patterns and down-tilting as well as height-dependent losses, cell sectorization, and drone fluctuations. Here, we report the formulation described in [6]

$$L_{PL}(l, l_j) = \alpha 10 \log_{10}(d) + \beta + X_\sigma \quad (2)$$

where d is the distance between the UAV and the BS location l_j , while α , β , and σ are the UAV's height-dependent path-loss exponent, the intercept point with the $d = 1$ m line, and the standard deviation of the normally distributed shadowing X , respectively. The reader is referred to [6] for further details. Last, let N be the Noise Power Spectral Density (NPSD). Accordingly, the uplink Signal-to-Interference-plus-Noise-Ratio (SINR) for user i served by cell j is denoted by $\text{SINR}_i = P^i / (NB_j + P_j^u \hat{x}_{ui})$. As we consider the uplink interference from ground UEs to the UAV negligible, the UAV's SINR can be calculated as $\text{SINR}_u = P^u / NB_u$. Consequently, the uplink achievable rate r_i of each user i is upper bound by the Shannon's capacity $C_i = B_i \log_2(1 + \text{SINR}_i)$ and is a function of the selected physical-layer coding and modulation scheme m_i [28]. In the Introduction of this article (§1), we illustrated a series of applications that rely on high-bandwidth connected drones to upload live videos of a specific Point of Interest (POI) over the cellular network. It is reasonable to think, thus, that one of the drone's application requirements is to be within the coverage area of the POI. Being POI a 3D location in space $\hat{l} \in \mathcal{L}$, it is an application-specific requirement for the UAV to respect a maximum distance dis_{\max} from the POI.

However, it is reasonable for the Internet Service Provider (ISP) to implement a two-step algorithm where the drone's serving cell is selected upon a given policy, as it happens for terrestrial users, and then solve the CDCP (7)-(10) for optimal drone location and transmission directionality. Last, we assume that the drone serving BS j_u is selected upon a given policy, as it happens for terrestrial users, and it is known at any given time. From a network optimization perspective, adopting the drone's location l and its transmission directionality δ as network control variables, the cellular CDCP can be formulated as follows:

$$\underset{l, \delta}{\text{maximize}} \quad r_u + \sum_{j \in \mathcal{J} / j_u} \sum_{i \in \mathcal{I}_j} r_i, \quad (3)$$

$$\text{subject to} \quad r_i > r_{\min}, \quad \forall i \in \mathcal{I} \quad (4)$$

$$r_u > r_{\text{app}}, \quad (5)$$

$$|l - \hat{l}| < \text{dis}_{\max}. \quad (6)$$

The CDCP problem formulated in (3)-(6) aims at maximizing the aggregate cellular users' uplink throughput. Specifically, the objective of CDCP is to maximize the total uplink data rates of all users that are co-scheduled (i.e., having an overlapping frequency band) with the UAV, including the UAV itself. Optimizing throughput for other users is outside the scope of this work. By maximizing the aggregate users' rate, the CDCP in (3)-(6) favors dense cells where users have limited band availability over the low populated cells where users have a wider band allocation. The rationale behind this design choice is two-fold. First, in the limited-band regime, limited-band users are more sensitive to performance drops caused by additional UAV interference due to their already limited data-rate. Second, limited-band users usually outnumber wide-band users. In solving the CDCP we consider not only the global network capacity but also the number of people that the drone might affect.

As an example, referring to Fig. 3b, the CDCP maximizes uplink rates of users i_2 and i_4 , which share their whole bandwidth with the interfering UAV, i.e., $\hat{x}_{iu} = 1$, together with the partially overlapping rate of users i_3 and i_5 ($0 < \hat{x}_{iu} < 1$). On the other hand, the rate of user i_6 , for which $\hat{x}_{iu} = 0$, is factored out of the CDCP, whereas rate of user i_1 is a constant of the CDCP and has been excluded from the formulation for this reason. Moreover, the CDCP prioritizes limited-band users, e.g., user i_4 and i_5 , over large-band users such as i_2 and i_3 . Together with the maximization function (3), we expressed constraints regarding the minimum per-user uplink QoS (4), the minimum UAV application-specific uplink data-rate (5), and the maximum distance with respect to a given POI (6). In other words, by selecting the optimal drone's location and its transmission directionality, the CDCP (3)-(6) tends to minimize the UAV impact on limited-band users who share a larger band portion with the UAV, while guaranteeing application-layer requirements to the drone.

The CDCP formulated in (3)-(6) is, however hard to solve for the following reasons:

(i) The time-varying, fine-grained information about x_i and m_i are determined by the BSs's MAC schedulers and PHY implementation which are often not exposed to a drone controller residing outside those BSs, due to transport overhead and/or proprietary PHY/MAC implementations [23].

(ii) Even though the latest development in the industry is pushing some PHY/MAC BS's control logic to be exposed to the north-bound controller (e.g., the Open-RAN Intelligence Controller [4]), the scheduling and rate-adaptation decisions are re-calculated in every transmission interval (e.g., 1 ms). It is therefore impossible for the drone to physically adapt its position and directionality to the instantaneous variation of x_i and m_i . As a result, the coefficients x_i and the modulations m_i in (3)-(6) are not only outside the control of the drone controller, but are non-observable.

(iii) In a real cellular network, ground users frequently relocate. Their mobility, even within the very same cell, changes their uplink signal strength at the serving BS at a fast pace. This makes their received power P^i and thus their uplink rate r_i in (3)-(6) change in real-time. Under this condition, the solver might calculate optimal solutions that, when implemented, do not reflect the current network state.

To address these challenges, we reformulate the CDCP in (3)-(6) by employing information that is changing at a relatively slower pace and is feasibly retrievable at the ISP in an Open-RAN architecture [4]. Specifically, we explore the network parameters that are described in the following.

Let \tilde{w}_j be long-run average number of users at cell j . This cell load information can be obtained at time intervals as short as 1 second, as currently done today between BSs when they need to exchange resource status. Accordingly, under a proportional fairness scheduler, each user served by BS j will be allocated a long-run average frequency resource equal to $\tilde{B}_j = B/\tilde{w}_j$. Then, let \tilde{P}_j be the aggregate uplink signal power received at BS j over band B in absence of UAVs. This is a slow-changing parameter that can be periodically retrieved by historical data, through the BSs' Application Programming Interface (API), or calculated using statistical per-cell users' distribution and the average cell load \tilde{w}_j . Accordingly, let us define the average UAV's uplink SINR at its serving BS j_u as $\widetilde{\text{SINR}}_u(l, \delta) = \frac{P^u(l, \delta)}{N\tilde{B}_u}$, where $P^u(l, \delta)$ is the received UAV signal power at the associated BS j_u that can be evaluated from the UAV location l and its transmission directionality δ . The average SINR for other users $i \in \mathcal{I}_u$ is defined as $\widetilde{\text{SINR}}_i = \frac{\tilde{P}_u}{N\tilde{B}_i}$ and is considered a constant of the CDCP. Similarly, the average uplink SINR for ground users served by BS $j \neq j_u$ is defined as $\widetilde{\text{SINR}}_j(l, \delta) = \frac{\tilde{P}_j}{N\tilde{B}_j + P_j^u(l, \delta)}$ where $P_j^u(l, \delta)$ is the received UAV interference power at the BS $j \neq j_u$, one more time, which is also a function of the UAV's location l and transmission directionality δ relative to the location of BS j . The CDCP can thus be reformulated as follows:

$$\underset{l, \delta}{\text{maximize}} \quad B_u \log_2 (1 + \widetilde{\text{SINR}}_u(l, \delta)) + \quad (7)$$

$$\sum_{j \in \mathcal{J}/j_u} B \log_2 (1 + \widetilde{\text{SINR}}_j(l, \delta)),$$

$$\text{subject to} \quad \widetilde{\text{SINR}}_j(l, \delta) > \text{SINR}_{\min} \quad \forall j \in \mathcal{J}/j_u, \quad (8)$$

$$\widetilde{\text{SINR}}_u(l, \delta) > \text{SINR}_{\text{app}}, \quad (9)$$

$$|l - \hat{l}| < \text{dis}_{\max}, \quad (10)$$

where (7) is the statistical average formulation of (3) and constraints (8)-(9) are the SINR-version of constraints (4)-(5). The CDCP in (7)-(10) is practically solvable and implementable thanks to the not

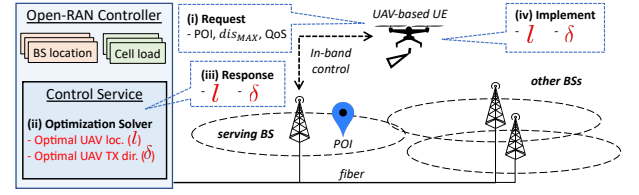


Figure 4: Proposed Open-RAN-based control system.

only observable, but easily retrievable network parameters at the ISP such as P^u , \tilde{P}_j , \tilde{w}_j , and \tilde{B}_u ; which catch the network average channel statistics and help us non-stationary avoiding the dependency on instantaneous rate terms in (3)-(6). Indeed, P^u and \tilde{P}_j can be calculated knowing the drone's location l and its transmission directionality δ , while the long-run average received uplink powers \tilde{P}_j , cell loads \tilde{w}_j , and the average users' band occupancy \tilde{B}_u are slow-changing parameters that can be estimated from ISP historical records, regularly reported by the BSs, or calculated using statistical ground users' geographical distribution. Ultimately, different from (3)-(6), the control parameters l and δ can be optimized and realized before the long-run statistics change. Should the network statistics change (e.g., network cell load shift) or the drone change its POI or its application-specific data-rate, the problem is to be solved once again for a new optimal solution.

Solving the CDCP. With the network parameters are retrievable in near-real-time (at time intervals as short as 1 second) [4], from an optimization standpoint, the CDCP (7)-(10) can be classified as a rugged funnel optimization problem [38]. In the presented scenario, the cardinality of the folds of the optimization function (i.e., the local minima) is represented by the number of neighboring cells impacted by the UAV-based UE interference. As the UE's output power is regulated by the standard (5G NR) and the interference is ultimately regulated by the path loss law, we have empirically verified that the number of local minima in the optimization function (7) is finite and bound. Most importantly, this number does not scale with the size or density of the deployment. In fact, as in commercial cellular networks the UEs' output power is regulated with the deployment density, and more aggressive path loss law counterbalance the deployment density at higher frequencies, the number of local minima is bound even in dense urban scenarios and in ultra-dense deployments at very-high-frequencies. This characterization guarantees that the CDCP (7)-(10) can be solved through a global convex optimization solver. Lastly, the proposed CDCP is flexible enough to address the stringent drone's application requirements, e.g., $\text{dis}_{\max} = 0$, or to solve for the best achievable drone QoS should the CDCP become infeasible, by progressively relaxing constraint (9).

4 CONTROL SYSTEM DESIGN

To realize the optimal solution obtained by solving the CDCP above, we envision here a control service that is integrated with the cellular network infrastructure and that has access to both static and real-time information from multiple eNBs within a market region through low-latency control links [16, 21]. Some static and real-time information that is relevant for our drone control service is cell configuration (e.g., antenna sector and frequency band) and cell load

(e.g., number of concurrent active users, averaged over every 1s interval), respectively. Such control implementation is architecturally consistent with several efforts in the O-RAN Alliance [4] that envisages a Radio Access Network Intelligent Controller (RIC) platform deployed by the cellular operator that will host such services [12].

The envisioned control system, as depicted in Fig. 4, is in charge of solving the CDCP formulated in Section 3 in near-real-time, that is based on the current state of the network, and relaying the computed solution to the drone over the same cellular links the drone is connected to, in an integrated-service-and-control fashion. The main operations of our control system are the following:

(i) The drone sends information to the control service about the POI's location, the application data-rate requirements, and the maximum tolerable distance from the POI (dis_{max}).

(ii) Based on the drone's requirements, coupled with the network information (cell load and topology), the Open-RAN control service computes the optimal solution (drone location, and drone's transmission directionality) by solving CDCP (7)-(10).

(iii) The service sends back the computed solution (drone's best location, and best transmission directionality) to the drone.

(iv) The drone (willingly) implements the computed optimal solution that guarantees the application data-rate and location requirements while minimizing its impact on the ground users.

(v) To cope with the changes in network load, the control service will periodically recalculate optimal solutions and communicate them to the drone. At the same time, if there are any application requirement changes (e.g., new data-rate and/or POI), the drone will send the updates back to the control service.

An illustration of our envisioned control loop architecture is shown in Fig. 4. The proposed control service design is beneficial for many reasons.

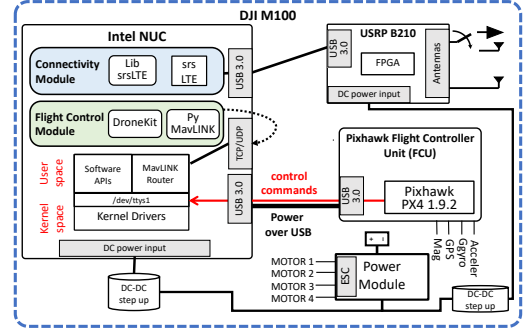
- *Backward compatibility*: The control service at the Open-RAN controller interacts with the drone in-band, that is over the same cellular links that are used for UE connectivity (e.g., the 5G data-link). This design choice eliminates the need for dedicated control links, Physical- or MAC layer modifications, and ultimately guarantees backward compatibility with the 5G standard stack.

- *Low Overhead*: Different than other interference mitigation schemes [19, 27], our approach is extremely lightweight. The information retrieved by the solver and the response to the drone can be encapsulated in only a few bytes of information. This property is beneficial for two reasons. Having low-overhead guarantees fast solution calculation and prompt implementation at the drone. Also, light signaling preserves the RAN stack functionality thus preventing channel saturation or undesirable delays.

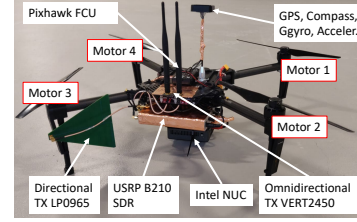
- *Users' privacy*: The proposed control approach is drone-initiated and guarantees aerial users' privacy. The drone voluntarily communicates its target POI and desired QoS to the service and implements the proposed solution, only if it is willing to do so. This way, no active trajectory control or motion tracking is performed by the service provider.

5 PERFORMANCE EVALUATION

In assessing the performance of the proposed control scheme, we start with an experimental evaluation on a full-stack, multi-cell LTE cellular network testbed. Our LTE-based analysis adopts the same



(a) UAV-based UE hardware schematics.



(b) UAV-based UE model.

Figure 5: UAV-based UE prototype

5G low- and mid-band frequencies suggested for drone cellular communications (FR1) [2]. To the best of our knowledge, this is the first real-world experiment of a connected-drone control system on a full-stack RAN testbed. Then, we extensively assess the performance of the proposed control scheme on a series of realistic large-scale deployments through simulation. In doing so, we utilize the commercial deployment topology and actual cell-load profile of a major US cellular carrier in several representative scenarios.

5.1 Small-scale Real-world Experiments

Experimental Setup. For our experiments, we prototype a multi-eNB LTE cellular network testbed using srsLTE which is an open-source, full-stack implementation of LTE for Software-Defined Radios (SDRs) [17, 31]. Our fully controllable LTE cellular testbed constitutes the following components.

- *Software stack*: The srsLTE suite comes with three modules, namely srsepc, srseNB, and srseUE, that implement the LTE-compliant protocol stacks for the core network, the eNB, and the UEs, respectively.
- *Host machines*: Each of the components above is hosted on an Intel NUC computer. The Intel NUC is a commercial Mini PC, whose compact dimensions and good computational capabilities (Intel Core i7 processor with 32 GB RAM) make it particularly suitable even to be carried on board of an UAV.
- *Radio front-ends*: We use the Universal Software Radio Peripheral (USRP) B210, a high-bandwidth, high-dynamic range SDR designed to operate from DC to 6 GHz frequency.

The deployment topology of our network consists of 3 eNBs covering 37500 ft² of outdoor space and a mixed set of 3 UEs as illustrated in Figs. 1, 2a, 2c, 6a, and 8a. In our deployments, each eNB serves one UE that is located approximately 25 ft away, with the eNBs located around 150 ft apart. The eNBs' antennas are placed

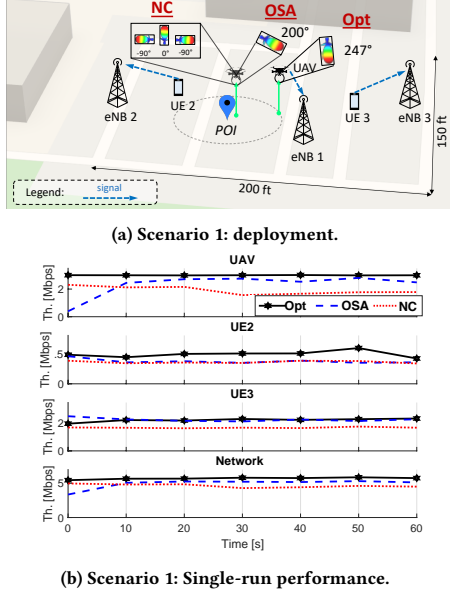


Figure 6: Network testing scenario 1.

at 10 ft from the ground using adjustable tripods, while the UE devices are placed at the ground level. Each eNB and UE uses a pair of antennas, VERT 2450, for transmission and reception over the air, whose radiation patterns can be found at [33]. Further, UE 1 is tethered to a UAV as shown in Fig. 5b. We designed and assembled a UAV-based UE by mounting a companion computer (Intel NUC) and a USRP B210 SDR on a DJI M100 drone. For the drone flight and motion control, we employed the Pixhawk flight controller board and the PX4 flight control firmware. Further, the drone can be alternatively equipped with a directional log-periodic LP0965 antenna as shown in Fig. 5b. The schematics of the prototyped aerial UE are illustrated in Fig. 5a. Lastly, to mimic the blockage and shadowing effect of typical cellular deployments in our experimental motivation section (see Sec. 2, Fig. 1) we use a large van positioned right behind the UAV. This way, the UAV will experience propagation patterns similar to traditional ground UEs when on the ground, that is, being in full LoS with at most one eNB only.

The 3-eNB network operates on LTE Band 7 where the uplink and downlink central frequencies are at 2535 MHz and 2655 MHz, respectively (which also corresponds to 5G NR band 7). To achieve a more robust testing deployment, we intentionally limit the operational bandwidth of the uplink and downlink directions to 3 MHz (15 PRBs). This reduces the pressure on SDR's host-based baseband processing, prevents user disassociation, and limits the interference to and from commercial cellular networks that operate on the same band. We reduce the complexity of our system by connecting a single UE to each of the eNBs. We induce saturated uplink traffic at each UEs so that each UE uses up all of the uplink PRBs from its serving eNB. To do so, we implement an iperf server at each eNB and an iperf client at each UE. We then select UDP over TCP as the transport protocol for its lack of congestion control which might interfere with our performance evaluation. This configuration is designed to mimic the uplink inter-cell interference conditions of a commercial cellular network in which multiple

UEs collectively occupy the whole spectrum band of their serving cells and create uplink inter-cell interference. In the following, we experimentally evaluate the effectiveness and adaptability of our proposed connected-drone control solution.

Effectiveness. In testing the proposed control solution we start from the deployment topology reported in Fig. 6. This consists of 3 eNBs – eNB 1, eNB 2, and eNB 3; and 3 UEs – the UAV, UE 2, and UE 3. Due to the dominant LoS conditions of our testing scenario, the users' serving cell is the nearest for all our experiments.

Herein, we assess the performance of the proposed Open-RAN-based control (Opt) against two other BS-constrained control schemes that, unable to access comprehensive RAN infrastructure information, target intra-cell users performance maximization. (i) *No Control* (NC), which adopts the POI as optimal drone location and a fixed transmission directionality. For this, we average the measurement across the 180° in the direction of the serving BS. (ii) *Optimal Serving Angle* (OSA), which envisions the drone hovering as close as possible to the Point of Interest (POI) and the directional transmitter pointing at the serving BS so as to maximize the application data-rate. For each control scheme, we measure the individual users' and the overall network performance.

In our experiment, the drone specifies a POI in between cell 1 and cell 2 demanding a maximum distance of 30 ft from it. For these scenarios, we specify a minimum drone's QoS of 2 Mbps. The deployment scenario for this experiment is illustrated in Fig 6a. We run a 1-minute long experiment for the proposed control scheme and the two baselines, and report the individual UEs throughput together with the aggregate network performance in Fig 6b. When adopting the Open-RAN-based control solution, the drone achieves higher throughput and overall better network performance as reported in Fig. 6b. Then, we run 10 1-minute long experiments for Scenario 1. The average performance results are reported in Fig. 7 (left). With the proposed control approach, the UAV, UE 2 and UE 3 achieve +0.69 Mbps, +0.14 Mbps, and -0.04 Mbps with respect to OSA, and +1.14 Mbps, +0.16 Mbps, and -0.13 Mbps with respect to NC. Overall, the network records +16% and +25% aggregated throughput gain with respect to OSA and NC.

Adaptability. When implementing the Open-RAN-based control solution, the drone can operate with the guarantee of satisfactory QoS and optimized network performance. This is true as long as the drone requirements stay the same (POI and QoS) and the network conditions are stationary. *What happens then when the stationary network conditions, e.g., the network cell load, change?* As mentioned earlier, upon statistical network load change, the Open-RAN-based control service, which continuously monitors the network conditions, calculates a new optimal operational point, and promptly communicates it to the drone. To induce a significant

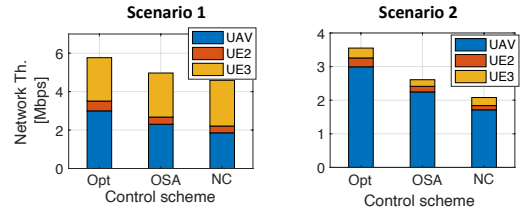


Figure 7: Average experimental performance results.

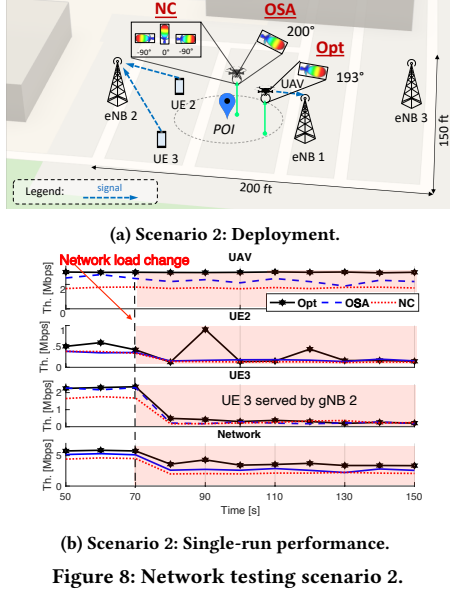


Figure 8: Network testing scenario 2.

change in cell load, we turn off a cell 3 user and turn one on in cell 2, thus emulating the move of UE 3 from one cell to another. This way, we double the load on eNB 2 and reduce the load on eNB 3 to zero. This perturbation emulates stationary geographical traffic shifts throughout the day, such as from business to residential districts after office hours.

With this experiment, we demonstrate how the proposed control approach adapts its solution to the network conditions to dynamically maximize the network throughput. Accordingly, we assess the performance of the two BS-constrained baselines NC and OSA on this new network configuration. Unlike the Open-RAN control solution, these control schemes are unable to implement a network-wide optimal policy, thus focusing on maximizing intra-cell performance and disregarding the interference implications on the rest of the network. Fig. 8 illustrates the new network deployment (Scenario 2) and the corresponding network performance analysis. By dynamically adapting to the network conditions, the proposed control scheme calculates and implements a new optimal solution that guarantees superior performance for both the UAV and the other ground UEs as reported in Fig. 8b. In this new scenario, the UAV, UE 2 and UE 3 achieve +0.53 Mbps, +0.1 Mbps, and +0.1 Mbps with respect to OSA, and +1.28 Mbps, +0.14, and +0.06 Mbps with respect to NC. Overall, the network records +36% and +52% throughput gain over OSA and NC. With an average cruise speed of 5 m/s, the drone only takes a few seconds to implement the new solution in this small network scenario. The long-running statistical network loads introduced in Section 3, however, guarantee fast convergence even in larger deployment scenarios.

Last, we are interested in quantifying the benefits of adopting a proactive, low-overhead, and low-latency control system that dynamically adapts to the changing network conditions in a closed-loop fashion. We quantify the performance toll paid by systems with complex information retrieval and reactive solution implementation typical, for example, of interference cancellation approaches relying on BS cooperation [19, 27]. We analyze the performance of a newly calculated optimal solution together with an outdated

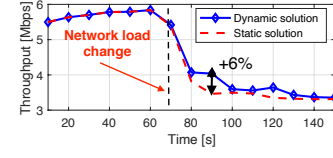


Figure 9: Performance toll for slowly-reacting control systems.

solution right after a change in the interference patterns, which can include a new cell load distribution, a new data-rate QoS, a new POI, or a combination of these. The latter is characteristic of a slowly-reacting control system. For this analysis, we factor out the optimization solver latency and the drone relocation time toward the new way-point. Fig. 9 reports a network throughput drop of 6% for adopting an outdated control problem solution after a network change. This drop translates into a 120 Mbps uplink throughput loss per second for a network at scale. This simple experimental evaluation highlights the benefits of employing a lightweight, low-overhead, and low-latency control system and suggests that more severe performance tolls might apply to slowly-reacting control systems in more complex cellular deployments.

5.2 Large-scale Simulation Analysis

Scalability. Here, we assess the scalability properties of our solution in large-scale, realistic deployment scenarios. For this task, we simulate three commercial deployment topologies of a major US cellular carrier: rural, suburban, and urban. These differ in terms of scale, cell distance, and cell deployment density. Additionally, we use the actual cell-load in terms of the average number of RRC connected UEs in a busy hour on the selected cells. An anonymized illustration of the three deployment scenarios is reported in the top part of Fig. 10. This assessment adds a high degree of realism to our evaluation and it is aimed at quantifying the gains of the proposed control approach on a real production network.

For our large-scale evaluation, we compare the performance of the Open-RAN-based control scheme (Opt) with NC, OSA, and two additional BS-constrained control schemes: i) *Optimal Serving Location* (OSL), which favors the drone's application data-rate by envisions the drone hovering as close as possible to the serving BS with a fixed transmission directionality (we average over the 180° in the direction of the serving BS); and ii) *Optimal Serving Location and Angle* (OSLA), which maximized the drone's application data-rate envisioning the drone hovering as close as possible to the serving BS with transmission direction pointing at the serving BS.

While the proposed Open-RAN-based solution (Opt) can employ network-wide deployment and cell-load information, the 4 BS-constrained control schemes (NC, OSA, OSL, OSLA) maximize intra-cell performances, unable to capture the impact on terrestrial users in the surrounding cells. For all the deployment scenarios, we assess the performance of the above control approaches for 20 different random POIs. In solving the CDCP for these realistic scenarios, we consider as drone's serving cell j_u the cell with one with strongest signal path according to published aerial channel models [6]. Further, we select a single carrier frequency and use commercial cell load profiles for a given band. The *anonymized*¹ cell load profile for the three deployments is the following. Rural:

¹Due to our NDA with the cellular carrier, we cannot report the actual cell load profile or cell deployment. For the sake of completeness, we however report similar cell load profiles and deployments per density and scale.

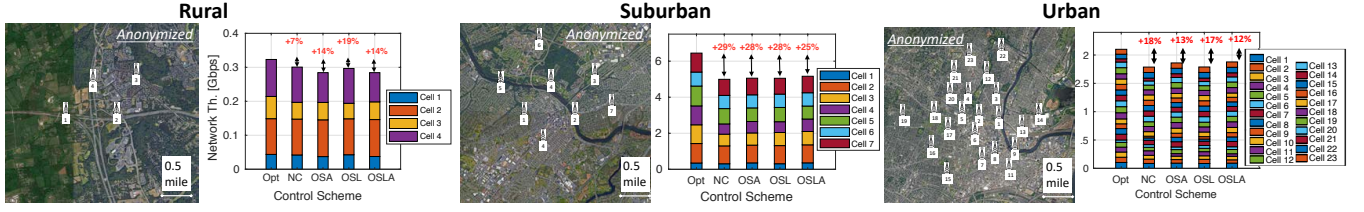


Figure 10: Anonymized¹ deployment topologies and performance analysis for the three large-scale scenarios.

57, 108, 36, 147 UEs; Suburban: 48, 135, 27, 36, 357, 261, 168 UEs; Urban: 120, 30, 21, 57, 129, 195, 60, 27, 54, 60, 126, 99, 75, 45, 30, 123, 90, 18, 90, 86, 33, 198, 78 UEs. Lastly, we express a hypothetical drone's QoS constraint of 5 Mbps (e.g., to support a 1080p and 60 fps stream), a maximum tolerable distance from POI of 500 ft, and a minimum SINR at the neighboring cells of 25 dB. We constrain the minimum drone's flight altitude according to the deployment's average building height (65 ft for rural and suburban, 165 ft for urban) and use a python solver (`scipy.minimize` suite) featuring global optimization capabilities to solve the CDCP. On a commercial machine, the solver takes less than 25 seconds to find a solution and the drone a few seconds to implement it as we have seen in our experiments. We expect even better performance on more powerful server machines or higher cruise speed. For each experiment, we measure the per-cell aggregate ground users' throughput and the overall compound network capacity (in Gbps). We report the average performance for the three scenarios and the 5 control schemes in Fig. 10 (bottom). The proposed Open-RAN-based control solution outperforms all the BS-constrained control schemes in all of the considered deployment scenarios. The proposed approach reports network capacity gains over the second-best performer as high as 23 Mbps, 128 Mbps, and 223 Mbps for rural, suburban, and urban deployments. These translate into an overall increased network capacity of 7%, 25%, and 12%. On average, the proposed control approach achieves +19% network capacity increase over the other network-agnostic control schemes on real, commercial network deployments, while satisfying target location and HQ video-streaming requirements to the drone.

6 RELATED WORK

While interference mitigation for exposed terminals in wireless networks is a well-studied subject [11, 22, 39], cellular-connected drones present some fundamental differences. A cellular-connected drone hovers at unprecedented and unprotected altitudes for a UE (different than pedestrians or users in tall buildings), it is highly-mobile (unlike users in hot air balloons or high up a hill), and its applications demand high data-rates (unlike high-altitude sensors). Thus, previous interference cancellation studies are hardly applicable to this scenario which remains under-explored. The difficulty of extending the ground-tailored wireless infrastructure to UAVs and the resulting A2G and ground-to-air (G2A) interference conditions have been highlighted in several works [8, 18, 24, 26, 30, 35, 37, 40]. Some produced propagation aerial models, setting the ground for future aerial network research [20, 32]. Some other works proposed interference mitigation solutions for cellular-connected UAVs. [19] proposed a multi-antenna interference cancellation for the downlink channel while [27] proposed a cooperative non-orthogonal

multiple access (NOMA) technique to mitigate the uplink interference at ground BSs. These approaches fail to provide a proactive solution for interference-prone A2G communications, leaving the burden of interference cancellation to complex reactive BS cooperation schemes. The use of directional transmitters at the UAVs is suggested in [7, 25] to improve both uplink and downlink communications. Directional transmission for UAV-based UEs is also proposed in [10], where Bertizzolo et. al. design a cooperative control mechanism to optimally control the trajectory and the orientation of the drone's transmission to mitigate the interference toward neighboring cells when the drone relocates from one way-point to another. These approaches focus on characterizing the benefits of directional transmitters and motion control without considering the specific bandwidth and application-specific requirements. On the other hand, other works have explored UAV location control for wireless network optimization outside the cellular paradigm [9, 14, 34, 36]. Unlike these works, we contextualize UAV-based UE broadband connectivity problem into the Open-RAN paradigm and approach it from an ISP's standpoint. Here, we exploit the architectural advantage of Open-RAN controllers to address the need for a drone-specific control solution that supports location and data-rate requirements for aerial video streaming applications.

7 CONCLUSIONS AND FINAL REMARKS

We introduced a new closed-loop control solution for Open RANs to support drone-based video streaming applications on commercial cellular networks. In our system, a UAV-based UE contacts a service at the Open-RAN controller for a satisfactory location and transmission directionality that support the application-specific location and QoS requirements. Exploiting the architectural advantage of Open-RAN controllers, the service computes and returns a solution that maximizes the overall network performance and matches the required QoS. The proposed approach features *backward compatibility*, *low overhead*, and *user privacy*. We assess the proposed solution on a real-world, outdoor, multi-cell RAN testbed. Further, we perform at-scale simulations employing the commercial cell deployment topologies and cell load profiles of a major US carrier. We prove *effectiveness* of the proposed control system (average 19% network capacity gain), *adaptability* to dynamic network conditions, and *scalability* to real-world deployments. We conclude this paper with a few final remarks.

Standard APIs. In this article, we proposed a control approach that is beneficial to the overall network, and which did not require any modification to the 5G protocol stack. Full integration of the proposed solution into commercial applications that guarantees the properties of low-overhead and user-privacy asks for standardized APIs. This will enable vendor-agnostic support and help the

development of drone-enabled cellular networks. Similarly, O-RAN compliant signaling procedures are needed for cell-load information retrieval.

Drone Mobility. To preserve users' privacy, the proposed solution does not implement mobility control or tracking. The implementation of the computed new location solution is instead left to the drone. This makes our approach, if you will, easily extendable and compatible with other trajectory control solutions and previous work on the subject, e.g., [10].

Directional Transmitters. Last, we care to remark that while this article limits its performance assessment to drones equipped with directional antennas, the proposed approach is directional transmitter-agnostic. While nowadays directional antennas are a more scalable and cost-effective solution for drones, the proposed approach will easily extend to antenna arrays, MIMO communications, and other more advanced forms of directional transmitters.

Future Work. Future research directions will model the aerial drone-to-drone interference to extend the current solution to multiple drone support. Accordingly, the current CDCP global optimization solver will have to be extended to support multi-drone optimization function.

REFERENCES

- [1] 2016. Amazon Prime Air. <https://www.amazon.com/Amazon-Prime-Air/b?ie=UTF8&node=8037720011>.
- [2] 2019. 3GPP TR 36.777, Enhanced LTE support for aerial vehicles. ftp://www.3gpp.org/specs/archive/36_series/36.777.
- [3] 2019. Eye in the sky. <https://www.shell.com/inside-energy/eye-in-the-sky.html>.
- [4] 2019. O-RAN RIC Specifications. <https://www.o-ran.org/specifications>.
- [5] 2020. Vodafone and Ericsson trial establishes automated flight paths for connected drones. <https://www.vodafone.com/news-and-media/vodafone-group-releases/news/vodafone-ericsson-safe-passage-drones>.
- [6] Rafael Amorim, Huan Nguyen, Preben Mogensen, István Z Kovács, Jeroen Wigard, and Troels B Sørensen. 2017. Radio channel modeling for UAV communication over cellular networks. *IEEE Wireless Commun. Lett.* 6, 4 (2017), 514–517.
- [7] Rafael Amorim, Huan Nguyen, Jeroen Wigard, István Z Kovács, Troels B Sørensen, David Z Biro, Mads Sørensen, and Preben Mogensen. 2018. Measured uplink interference caused by aerial vehicles in LTE cellular networks. *IEEE Wireless Communications Letters* 7, 6 (2018), 958–961.
- [8] Mohammad Mahdi Azari, Fernando Rosas, Alessandro Chiumento, and Sofie Pollin. 2017. Coexistence of terrestrial and aerial users in cellular networks. In *2017 IEEE Globecom Workshops (GC Wkshps)*.
- [9] Lorenzo Bertizzolo, Salvatore D'oro, Ferranti Ludovico, Leonardo Bonati, Emrecan Demirs, Zhangyu Guan, Tommaso Melodia, and Scott Pudlewski. 2020. SwarmControl: An Automated Distributed Control Framework for Self-Optimizing Drone Networks. In *Proc. of IEEE Conference on Computer Communications (INFOCOM)*. 1768–1777.
- [10] Lorenzo Bertizzolo, Tuyen X. Tran, Brian Amento, Bharath Balasubramanian, Rittwik Jana, Hal Purdy, Yu Zhou, and Tommaso Melodia. 2020. Live and Let Live: Flying UAVs Without Affecting Terrestrial UEs. In *Proc. of the 21st Intl. Workshop on Mobile Computing Systems and Applications (HotMobile)*. Austin, TX, USA.
- [11] Leonardo Bonati, Salvatore D'Oro, Lorenzo Bertizzolo, Emrecan Demirs, Zhangyu Guan, Stefano Basagni, and Tommaso Melodia. 2020. CellOS: Zero-touch Softwarized Open Cellular Networks. *Computer Networks* 180 (June 2020).
- [12] Leonardo Bonati, Michele Polese, Salvatore D'Oro, Stefano Basagni, and Tommaso Melodia. 2020. Open, Programmable, and Virtualized 5G Networks: State-of-the-Art and the Road Ahead. *Computer Networks* (2020).
- [13] Ahmed Boubrima and Edward W Knightly. 2020. Robust mission planning of UAV networks for environmental sensing. In *ACM Workshop on Micro Aerial Vehicle Networks, Systems, and Applications (DroNet)*. 2–1.
- [14] Ayon Chakraborty, Eugene Chai, Karthikeyan Sundaresan, Amir Khojastepour, and Sampath Rangarajan. 2018. SkyRAN: A self-organizing LTE RAN in the sky. In *Proceedings of the 14th International Conference on emerging Networking Experiments and Technologies*. 280–292.
- [15] CNN. 2020. CNN cleared to test drones for reporting. Technical Report. <https://money.cnn.com/2015/01/12/technology/cnn-drone/>.
- [16] Liljana Gavrilovska, Valentin Rakovic, and Daniel Denkovski. 2020. From Cloud RAN to Open RAN. *Wireless Personal Communications* (2020), 1–17.
- [17] I. Gomez-Miguel, A. Garcia-Saavedra, P.D. Sutton, P. Serrano, C. Cano, and D.J. Leith. 2016. srsLTE: An Open-source Platform for LTE Evolution and Experimentation. In *Proc. of ACM WiTECH*. New York City, NY, USA, 25–32.
- [18] William D Ivancic, Robert J Kerczewski, Robert W Murawski, Konstantin Mathieu, and Alan N Downey. 2019. Flying Drones Beyond Visual Line of Sight Using 4g LTE: Issues and Concerns. In *2019 Integrated Communications, Navigation and Surveillance Conference (ICNS)*.
- [19] Tomasz Izydorczyk, Mădălina Bucur, Fernando ML Tavares, Gilberto Berardinelli, and Preben Mogensen. 2018. Experimental evaluation of multi-antenna receivers for UAV communication in live LTE networks. In *2018 IEEE Globecom Workshops*.
- [20] Aziz Altaf Khuwaja, Yunfei Chen, Nan Zhao, Mohamed-Slim Alouini, and Paul Dobbins. 2018. A survey of channel modeling for UAV communications. *IEEE Communications Surveys & Tutorials* 20, 4 (2018), 2804–2821.
- [21] Edwin J Kitindi, Shu Fu, Yunjian Jia, Asif Kabir, and Ying Wang. 2017. Wireless network virtualization with SDN and C-RAN for 5G networks: Requirements, opportunities, and challenges. *IEEE Access* 5 (2017), 19099–19115.
- [22] Sunil Kumar, Vineet S Raghavan, and Jing Deng. 2006. Medium access control protocols for ad hoc wireless networks: A survey. *Ad hoc networks* 4, 3 (2006), 326–358.
- [23] Line MP Larsen, Aleksandra Checko, and Henrik L Christiansen. 2018. A survey of the functional splits proposed for 5G mobile crosshaul networks. *IEEE Communications Surveys & Tutorials* 21, 1 (2018), 146–172.
- [24] Xingqin Lin, Vijaya Jayananarayana, Siva D Muruganathan, Shiwei Gao, Henrik Asplund, Helka-Liina Maattanen, Mattias Bergstrom, Sebastian Euler, and Y-P Eric Wang. 2018. The sky is not the limit: LTE for unmanned aerial vehicles. *IEEE Magazine* 56, 4 (2018), 204–210.
- [25] Jiangbin Lyu and Rui Zhang. 2017. Blocking probability and spatial throughput characterization for cellular-enabled UAV network with directional antenna. *arXiv preprint arXiv:1710.10389* (2017).
- [26] Weidong Mei, Qingqing Wu, and Rui Zhang. 2019. Cellular-connected UAV: Uplink association, power control and interference coordination. *IEEE Transactions on Wireless Communications* (2019).
- [27] Weidong Mei and Rui Zhang. 2019. Uplink cooperative NOMA for cellular-connected UAV. *IEEE J. Sel. Topics in Sig. Processing* 13, 3 (2019), 644–656.
- [28] Preben Mogensen, Wei Na, István Z Kovács, Frank Frederiksen, Akhilesh Pokhariyal, Klaus I Pedersen, Troels Kolding, Klaus Hugel, and Markku Kuusela. 2007. LTE capacity compared to the Shannon bound. In *2007 IEEE 65th vehicular technology conference-vtc2007-spring*. IEEE, 1234–1238.
- [29] Syed Ahsan Raza Naqvi, Syed Ali Hassan, Haris Pervaiz, and Qiang Ni. 2018. Drone-aided Communication as a Key Enabler for 5G and Resilient Public Safety Networks. *IEEE Communications Magazine* 56, 1 (2018), 36–42.
- [30] Huan Cong Nguyen, Rafael Amorim, Jeroen Wigard, István Z Kovács, Troels B Sørensen, and Preben E Mogensen. 2018. How to ensure reliable connectivity for aerial vehicles over cellular networks. *IEEE Access* 6 (2018), 12304–12317.
- [31] Navid Nikaein, Raymond Knopp, Florian Kaltenberger, Lionel Gauthier, Christian Bonnet, Dominique Nussbaum, and Riadh Ghaddab. 2014. OpenAirInterface: an open LTE network in a PC. In *Proc. of International Conference on Mobile Computing and Networking*. Maui, HI, USA, 305–308.
- [32] Michele Polese, Lorenzo Bertizzolo, Leonardo Bonati, Abhimanyu Gosain, and Tommaso Melodia. 2020. An Experimental mmWave Channel Model for UAV-to-UAV Communications. In *Proc. of 4th ACM Workshop on Millimeter-wave Networks and Sensing Systems (mmNets)*. London, UK.
- [33] Ettus Research. 2020. Vert2450. https://kb.ettus.com/images/9/9e/ettus_research_vert2450_datasheet.pdf.
- [34] Ramanujan K Sheshadri, Eugene Chai, Karthikeyan Sundaresan, and Sampath Rangarajan. 2020. SkyHaul: An Autonomous Gigabit Network Fabric in the Sky. *arXiv preprint arXiv:2006.11307* (2020).
- [35] Jędrzej Stanczak, Istvan Z Kovacs, Dawid Koziol, Jeroen Wigard, Rafael Amorim, and Huan Nguyen. 2018. Mobility challenges for unmanned aerial vehicles connected to cellular LTE networks. In *2018 IEEE 87th Vehicular Technology Conference (VTC Spring)*.
- [36] Karthikeyan Sundaresan, Eugene Chai, Ayon Chakraborty, and Sampath Rangarajan. 2018. SkyLiTE: End-to-end design of low-altitude UAV networks for providing LTE connectivity. *arXiv preprint arXiv:1802.06042* (2018).
- [37] Bertold Van der Bergh, Alessandro Chiumento, and Sofie Pollin. 2016. LTE in the sky: Trading off propagation benefits with interference costs for aerial nodes. *IEEE Communications Magazine* 54, 5 (2016), 44–50.
- [38] Massimiliano Vasile, Edmondo Minisci, and Marco Locatelli. 2010. Analysis of some global optimization algorithms for space trajectory design. *Journal of Spacecraft and Rockets* 47, 2 (2010), 334–344.
- [39] Robert Vilzmann and Christian Bettstetter. 2006. A survey on MAC protocols for ad hoc networks with directional antennas. In *EUNICE 2005: Networks and Applications Towards a Ubiquitously Connected World*. Springer, 187–200.
- [40] Yong Zeng, Jiangbin Lyu, and Rui Zhang. 2018. Cellular-connected UAV: Potential, challenges, and promising technologies. *IEEE Wireless Communications* 26, 1 (July 2018), 120–127.